Biomimetic Ultrathin Whitening by Capillary-Force-Induced Random Clustering of Hydrogel Micropillar Arrays

Dinesh Chandra,[†] Shu Yang,*,[†] Andre A. Soshinsky,[‡] and Robert J. Gambogi[§]

Department of Materials Science and Engineering, University of Pennsylvania, 3231 Walnut Street, Philadelphia, Pennsylvania 19104, Johnson and Johnson Consumer Products, 185 Tabor Road, Morris Plains, New Jersey 07950, and Johnson and Johnson Consumer Products, 199 Grandview Road, Skillman, New Jersey 08558

ABSTRACT Capillary-force-induced collapse of high-aspect-ratio microstructures has often been considered a failure mechanism in device fabrication. Here, we study capillary-force-induced clustering behavior of highly ordered hydrogel micropillar arrays from 2-hydroxyethyl methacrylate (HEMA) and methyl methacrylate (MMA) and explore their utility as ultrathin whitening layers (less than 9 μm thick). When exposed to water, followed by drying in an air stream, the micropillars were softened, bent, and randomly clustered together because of competition between the capillary force and elastic restoring force of the pillars. By varying the relative composition of the water-swellable PHEMA and glassy PMMA, we modulated the elastic modulus of the pillars in the wet state spanning over 3 orders of magnitude. By minimizing the sum of the capillary meniscus interaction energy and the elastic bending energy of the pillars for a cluster, we estimated the average cluster size as a function of the elastic modulus of the pillars, which agreed well with the experimental observation. The randomly clustered micropillar arrays appeared white in color because of random light scattering from the clusters, similar to the observation in the white beetles, whose scales consist of a few micrometer-thick random networks of microfilaments.

KEYWORDS: micropillar • biomimetic • ultrathin whitening • capillary force • clustering

INTRODUCTION

High-aspect-ratio micropillar arrays play an important role in a wide range of applications, including superhydrophobic surfaces and tunable wetting (1−3), force sensing and actuation (4, 5), dry adhesives (6), tissue engineering (4, 5), and filtration and separation (7). However, because of their small effective stiffness, high-aspect-ratio structures tend to deform under external forces. Recently, such structural collapse has been harnessed to induce the spontaneous formation of helicity for particle trapping (8). Previously, we have reported the fabrication of stable high-aspect-ratio (height-to-diameter ratio up to 20) epoxy micropillar arrays in air (9). However, many applications for tall micropillar arrays require them to be used in a liquid environment, where the combination of a decreased elastic modulus of the pillars due to swelling and the capillary force during drying could adversely cause them to collapse (10−12). On the other hand, the capillary force has been utilized, for example, to form carbon nanotube foams (13) and to self-assemble superstructures (8, 10, 14). One important question is whether we can predict the clustering behavior of high-aspect-ratio pillars due to capillary force, which will be important to the utilization of a capillary-driven self-assembly process.

Here, we report both theoretical and experimental studies of the clustering behavior of hydrogel micropillar arrays with well-defined geometries induced by capillary force and their utility as biomimetic ultrathin whitening layers. By varying the composition of the water-swellable 2-hydroxyethyl-methacrylate (PHEMA) component versus the glassy, non-swellable methyl methacrylate (PMMA) as the micropillar material, we systematically modulated the effective elastic modulus of the micropillars from poly(2-hydoxylmethacrylate-co-methyl methacrylate) (PHEMA-co-PMMA) in the wet state over 3 orders of magnitude. The ability to tune the elastic modulus of the micropillars over a wide range allowed us to experimentally study the effect of the elastic modulus on clustering. Clustering of macroscopic fibers when withdrawn from a liquid bath has been studied previously in terms of the balance between the elastic bending energy and capillary energy (15, 16). It is important to point out that in these studies the capillary energy due to clustering originated from a reduction in the liquid−vapor surface area along a part of the fiber length withdrawn from the liquid. However, in the case of micropillar clustering during liquid evaporation, the relevant capillary energy is the interaction energy of the liquid menisci (17) surrounding the micropillars, while the latter are still immersed in the liquid except at the tip (Figure 3a-ii). Few have systematically investigated micropillar clustering by considering the meniscus interaction energy. Here, by minimizing the sum of the capillary meniscus interaction energy and the elastic bending energy of

the micropillars, we quantitatively predicted the average cluster size as a function of the elastic modulus of the pillar materials, which agreed well with the experimental observation. Further, we demonstrated that such random clustering of micropillar arrays could be utilized to design ultrathin whitening layers, mimicking the whiteness in ultrathin white beetle scales (18).

EXPERIMENTAL METHODS

Materials. HEMA (98 %) and MMA (99 %) monomers were obtained from Aldrich and Acros Organics, respectively. Cross-linker ethylene glycol dimethacrylate (EGDMA) (98 %) was obtained from Alfa Aesar. Photoinitiator Darocur 1173 was obtained from Ciba Specialty Chemicals Inc. The PDMS precursor and curing agent (Sylgard 184) was obtained from Dow Corning. All of the chemicals were used without further purification.

Fabrication of Micropillar Arrays. The micropillar arrays were fabricated by a two-step replica molding process, as described in our earlier publication (10). Two types of micropillar arrays were investigated, including geometry A (a pillar diameter of 0.75 μm and a pitch of 1.5 μm) and geometry B (a pillar diameter of 1 μm and a pitch of 2 μm), both of which were 9 μm tall, and the diameter/pitch ratios were kept the same in both geometries. In a typical procedure, 2.5 mL of a monomer mixture of HEMA and MMA was mixed with 75 μL of Darocur 1173 and exposed to UV light (UVP Blak-Ray, ~8 mW/cm^2) for 2 min (5 min for MMA $\geq$ 60 wt %) to obtain a viscous partially polymerized precursor solution. Before molding, an additional 50 μL of Darocur 1173 and 25 μL of EGDMA were added to this solution to prepare the molding precursor. PDMS molds were prepared by mixing a PDMS precursor and curing agent in a 10:1 ratio by weight and pouring it on a silicon micropillar arrays master followed by curing at 65 °C for 4 h. The cured molds were then carefully peeled off the silicon master. To fabricate the hydrogel micropillar arrays, the molding solution was cast on a silicon wafer and the PDMS mold was pressed over it, followed by UV exposure by a 97435 Oriel Flood Exposure Source (Newport Corp.) at a dose of 7200 mJ/cm^2. To collapse the micropillars to form clusters, the micropillar arrays were soaked in water for 10 min, followed by drying in an air stream. The volume of the introduced water was kept the same during all experiments.

Average Cluster Size Determination. Clustered micropillar arrays were imaged by scanning electron microscopy (SEM; FEI Strata DB235 Focused Ion Beam) at an acceleration voltage of 5 kV and a spot size of 3. The samples were sputter-coated with platinum before imaging. The cluster size was determined by manually counting the number of pillars in the individual clusters and reported as the average and standard deviation for all clusters in an area of 0.02 mm^2 from SEM images.

Water Contact-Angle Measurement. Static contact angles on flat PHEMA-*co*-PMMA films were measured using a Ramé-Hart goniometer with DROPimage Advanced software. Reported values were averaged over at least five different spots. The water drops used were ~1.5 μL in volume.

Elastic Modulus Measurement. Elastic moduli of wet PHEMA-*co*-PMMA films were measured by atomic force microscopy (AFM) nanoindentation (19−21) under water in a fluid cell using a Digital Instruments Multimode atomic force microscope. The indentation force curves (cantilever deflection d vs piezo displacement z; see Figure S1a in the Supporting Information) were analyzed by a method outlined by Domke and Radmacher (20). The zero deflection point d_0 of the cantilever was determined from the noncontact part of the force curve (Figure S1a in the Supporting Information). The force applied by the cantilever tip on the film is

$$F = k(d - d_0) \qquad (1)$$

where k is the spring constant of the cantilever, which was determined by the resonant frequency method as described by Sader et al. (22). Two types of cantilevers were used: soft cantilevers ($k \approx 0.1$ N/m) for soft samples with MMA content $\leq$25 wt % and stiffer cantilevers ($k \approx 20$ N/m) for samples with a higher MMA content. The indentation depth is defined by $\delta = (z - z_0) - (d - d_0)$, where z_0 is the contact point (Figure S1 in the Supporting Information). According to the conical tip approximation, the relationship between indentation δ and force F is given as (20, 23),

$$F = (2/\pi)[E/(1 - v^2)]\delta^2 \tan \alpha \qquad (2)$$

where E is the elastic modulus, v is Poisson's ratio (here assumed to be 0.5 20, 21), and α is the half opening angle of the cantilever tip, which was determined as 18° from SEM imaging. From eqs 1 and 2,

$$z - d = (z_0 - d_0) + (d - d_0)^{1/2} \sqrt{\frac{\pi k(1 - v^2)}{2E \tan \alpha}} \qquad (3)$$

Equation 3 suggests a linear relationship between $z - d$ and $(d - d_0)^{1/2}$. Therefore, the elastic modulus E was determined from the slope of $z - d$ versus $(d - d_0)^{1/2}$ (Figure S1b in the Supporting Information). The reported elastic moduli represent the average over indentations at three to seven different spots for each sample.

Whiteness Characterization. The whiteness of the clustered micropillar arrays was characterized by measuring their CIE lightness index, L, specified by International Commission on Illumination (24), using a photospectrometer (MHT Spectro Shade Micro). L represents the diffuse reflectance of a surface on a scale from 0 to 100, where 0 is black and 100 is perfect white. The reported data represent the average lightness index for three different samples with a small (less than 1) standard deviation.

RESULTS AND DISCUSSION

Micropillar Clustering by Capillary Force. Two types of hydrogel micropillar arrays were fabricated by replica molding of partially polymerized copolymer precursors from HEMA and MMA, followed by photo-cross-linking (see details in the Experimental Methods). The micropillar arrays were then soaked in water and dried in a stream of air to collapse the pillars to include clustering (Figure 1). Because PMMA is a glassy polymer ($T_g \sim 100$ °C) and does not absorb water whereas PHEMA does, we can systematically vary the composition of HEMA and MMA in the molding precursor, thus controlling the degree of hydration and the effective elastic modulus of the micropillars in the wet state (Figure 2a). As shown in Figure 1, the micropillar cluster size decreases with an increase in the PMMA content, and thus an increase in the elastic modulus (Figure 2a). For a given PMMA content, the cluster size from a type A micropillar array was typically larger than that from a type B array because A had a smaller pillar diameter (0.75 μm) and a higher aspect ratio (12) than those of B (a pillar diameter of
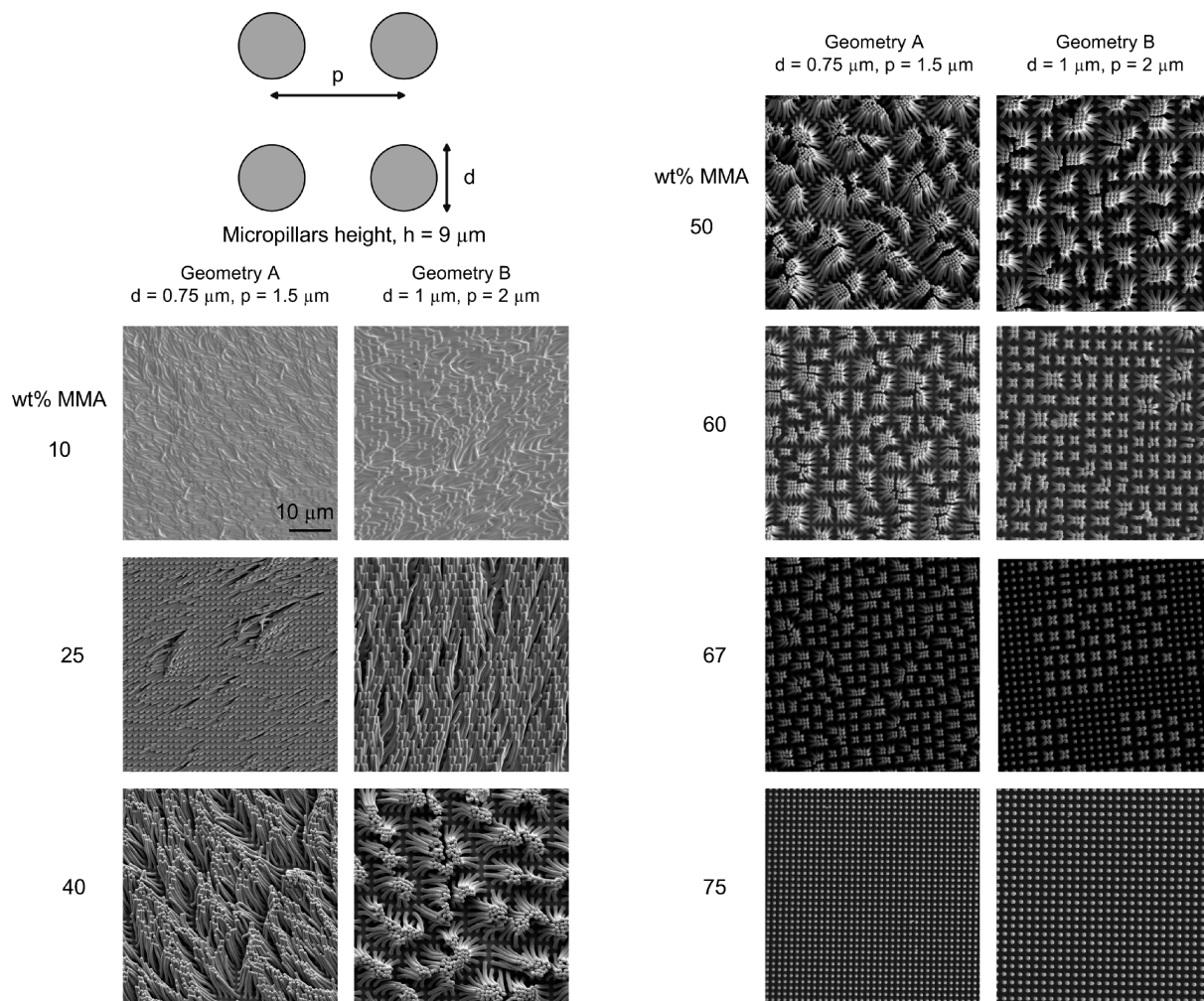
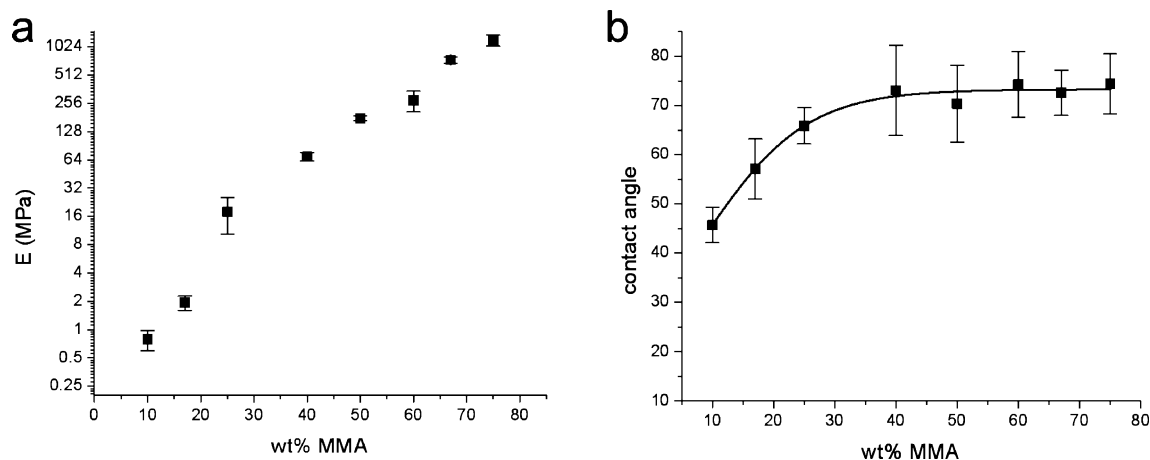FIGURE 1. SEM images of 9-μm-tall PHEMA-*co*-PMMA micropillar arrays clustered by a water capillary force.

FIGURE 2. Elastic modulus in the wet state (a) and the water contact angle (b) of flat PHEMA-*co*-PMMA films as a function of the MMA content.

1 μm and an aspect ratio of 9, respectively). In both geometries, the diameter/pitch ratio was kept the same.

When the micropillar arrays were soaked in water, the pillars softened because of water absorbed by PHEMA, resulting in a smaller effective elastic modulus in the wet sate, which was dependent on the relative composition of PHEMA and PMMA. When the micropillar arrays soaked in water (Figure 3a-i) were dried by air flow, liquid menisci

were formed around the individual pillars (Figure 3a-ii). We think the interaction between these liquid menisci exerted an attractive force (17) between the micropillars, causing them to cluster together while still surrounded by water (Figure 3a-iii). To investigate the possible contribution of the volume change during the drying process to pillar deformation, we soaked the bulk films of the same composition in water. The results suggested that the volume change in the

samples was negligible. However, because of the elastoplastic nature of the hydrogel films and the strong adhesive force between the clustered pillars, the deformation became permanent and the pillars could not spring back after the water was completely dried (Figure 3a-iv). At very low PMMA content (<25 wt %), the micropillars are very soft (Figure 2a), resulting in the ground collapse (9) of micropillars (Figure 1), which could be attributed to gravity, an increase of the capillary force during drying, or a combination of the two.

Calculation of the Cluster Size. The effect of the elastic modulus on the cluster size can be understood in terms of the balance between the capillary energy and elastic bending energy of a cluster. When the micropillar array is exposed to a wetting liquid, followed by liquid evaporation, the capillary meniscus interaction force of the liquid menisci surrounding the micropillars will pull the micropillars to collapse into clusters. Because the bases of the pillars are attached to the substrate, the pillars have to bend, which increases the elastic bending energy of the cluster. As the pillars come closer together, the capillary meniscus interaction energy of the cluster decreases. The maximum number of pillars in a cluster is the result of the competition between the total bending energy and the total capillary energy of the cluster. Qualitatively, in a cluster, the outer pillars have to bend more than the inner pillars. As shown later, this causes the positive bending energy to scale roughly as N^2, where N is the number of pillars in a cluster. However, the decrease in the capillary energy per pillar in a cluster is the same for all pillars. Thus, the negative capillary energy scales as N. The difference in scaling of the positive bending energy and negative capillary energy results in a minimum energy for a critical cluster size, N_c. The bending energy of a rod, which is fixed at one end, of radius r, length h, and elastic modulus E, is given as (25),

$$\Delta E_b = \frac{3\pi E r^4 \delta^2}{8h^3} \tag{4}$$

where δ is the displacement of the free end of the rod. Because of the symmetry of the underlying square lattice, the micropillars in a cluster also pack into a square lattice in general (Figure 3c). The total bending of a cluster packed into a square lattice (Figure 3b) can be viewed as the sum of bending of perimeters $n = 1, 2, 3, 4, ...,$ i.e., $\delta^2 = \Sigma \delta_n^2$. Cumulative bending in perimeter n can be obtained as

$$\delta_n^2 = 4\left(\frac{s}{2}\right)^2[(2n-1)^2 + (2n-1)^2] + 8\left(\frac{s}{2}\right)^2 \sum_{i=1}^{n-1}[(2n-1)^2 + (2i-1)^2] \tag{5}$$

where the first term represents the bending of four corner pillars and the second term represents the bending of the remaining $8(n-1)$ pillars in perimeter n. Here, s is the separation of the pillars (Figure 3b). Thus, the total bending of a cluster having n perimeters is

$$\delta^2 = \sum \delta_n^2 = \frac{s^2}{3}(8n^4 - 2n^2 + 6n - 6) \tag{6}$$

From eqs 4 and 6, the total elastic bending energy is given as

$$U_e = \frac{\pi E r^4 s^2 (8n^4 - 2n^2 + 6n - 6)}{8h^3} \tag{7}$$

Here the total number of pillars in a cluster, N, is given by $N = 4n^2$. Because in eq 7 U_e roughly scales as $\sim n^4$, $U_e \sim N^2$, as mentioned earlier.
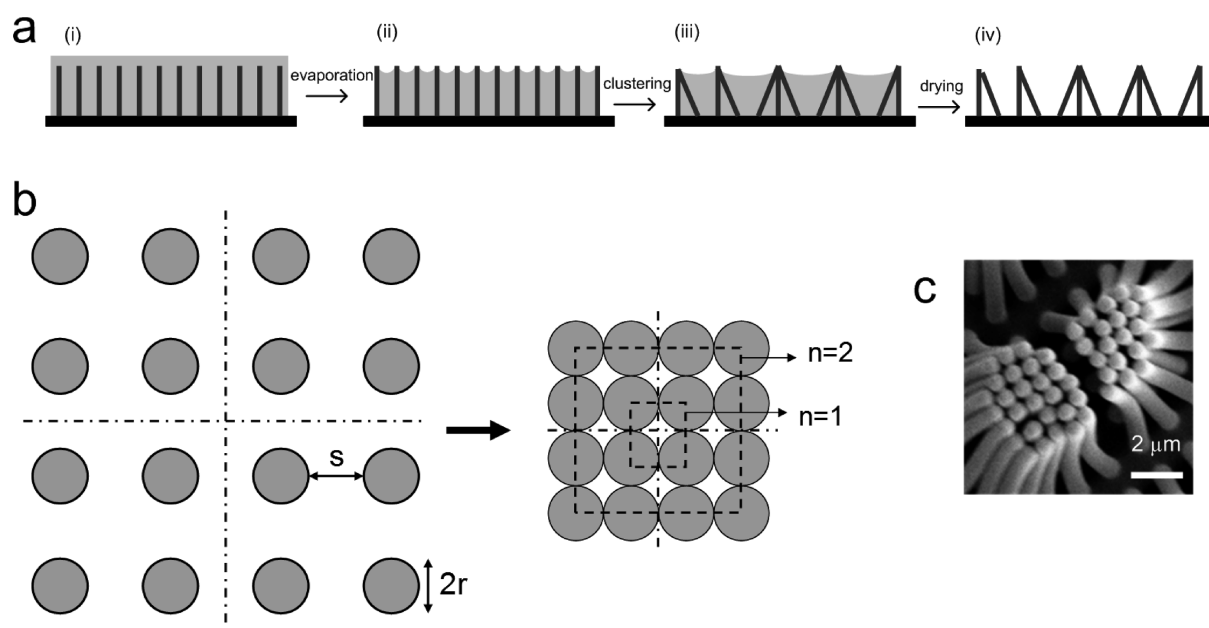

FIGURE 3. (a) Schematic illustration of micropillar clustering process due to a capillary meniscus interaction force. (b) Schematic illustration of micropillar array clustering in a square lattice. (c) SEM image of micropillars clustered in a square lattice.

The capillary energy of two vertical cylindrical rods of radius r and separated by center-to-center distance $2l$ partially submerged in a liquid is given as (17)

$$W = 2\pi\gamma r^2 \cos^2 \theta \left(\ln \frac{(a+l)\gamma_e q}{1+\sin\theta} \right) \quad (8)$$

where γ is the surface tension of the liquid and θ is the liquid contact angle on the rod material. Here, $a = (l^2 - r^2)^{1/2}$, γ_e is the Euler–Maceroni number ($\gamma_e = 1.78107$), and $q^{-1} = (\gamma/\rho g)^{1/2}$ is the capillary length, where ρ is the density of the liquid and g is the gravitational acceleration. Each pillar is surrounded by eight pillars, including four corner pillars [center-to-center distance $2^{1/2}(2r+s)$ when not collapsed and $2(2^{1/2})(r)$ when collapsed] and four adjacent pillars [center-to-center distance $2r+s$ when not collapsed and $2r$ when collapsed; see Figure 3b]. For both geometries A and B, $s = 2r$. Thus, by eq 8, the total change in the capillary meniscus interaction energy from the noncollapsed to collapsed state (Figure 3a) of a cluster with n perimeters is calculated as

$$U_c = -4\pi\gamma r^2 \cos^2 \theta \left((4n^2 - 2n)\ln(\sqrt{3}+2) + (4n^2 - 4n + 1)\ln\left(\frac{\sqrt{7}+2\sqrt{2}}{\sqrt{2}+1}\right) \right) \quad (9)$$

In eq 9, the first logarithmic term represents the capillary energy due to adjacent pillars, whereas the second term represents that due to the corner pillars. The negative terms account for the fact that the outermost pillars in a cluster are surrounded by less than eight pillars. Further, we note that in the derived eq 9 the change in the capillary meniscus interaction energy is independent of the capillary number q.

Thus, the total energy of formation of a cluster is $U_t = U_c + U_e$. Minimization of the total energy by $\partial U_t/\partial n = 0$ gives
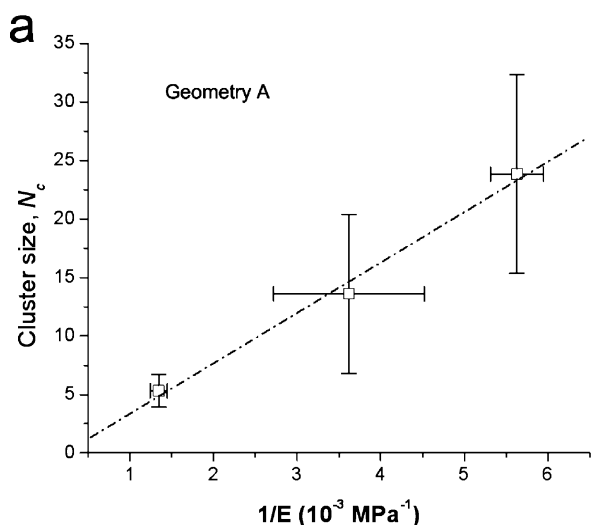
$$E = \frac{32\gamma \cos^2 \theta h^3}{r^2 s^2} \times$$
$$\left(\frac{(8n_c - 2)\ln(\sqrt{3}+2) + (8n_c - 4)\ln\left(\dfrac{\sqrt{7}+2\sqrt{2}}{\sqrt{2}+1}\right)}{32n_c^3 - 4n_c + 6} \right) \quad (10)$$

where the number of pillars in a cluster $N_c = 4n_c^2$. Numerically solving eq 10 in terms of N_c reveals a linear relationship (eq 11) between N_c and $1/E$ (see Figure S2 in the Supporting Information). The linear relationship can also be inferred by neglecting the numerical constants in the polynomials containing n_c in eq 10 and then solving analytically for N_c.

$$N_c \approx \frac{64.51 \cos^2 \theta \gamma h^3}{E r^2 s^2} - 2.11 \quad (11)$$

Previously, Zhao and Fan (26) predicted that the cluster size was dependent on gravity through the capillary length q^{-1}. However, eqs 10 and 11 suggest that gravity should not be relevant to the change in the capillary interaction energy where the cluster size is independent of q. From eq 11, the cluster size is inversely proportional to the elastic modulus of the micropillars with a slope of $(64.51\gamma \cos^2 \theta h^3)/r^2 s^2$. To validate the above relationship, we compared the experimentally observed cluster size to the prediction according to eq 11. The elastic modulus E was experimentally determined by AFM nanoindentation of PHEMA-co-PMMA samples immersed in water (Figure 2a). The measured water contact angle θ in eq 11 was found to increase with an increase in the MMA weight percent initially but leveled off at ~73° when MMA content ≥ 40 wt % (Figure 2b).

In Figure 4, we plotted experimentally observed values of N_c versus $1/E$ for both pillar array geometries. The vertical error bars represent the standard deviation of the cluster sizes in a sample, and the horizontal error bars represent the error in the elastic modulus measurement. The dashed
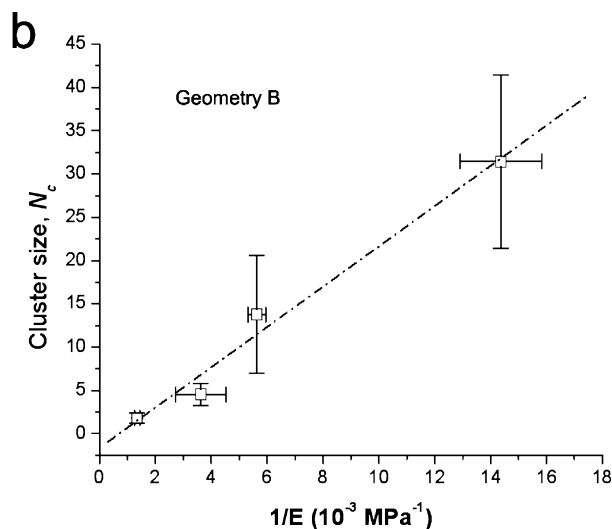

FIGURE 4. Micropillar cluster size as a function of the elastic modulus of micropillars in the wet state for (a) geometry A and (b) geometry B. The dashed lines are the linear fit ($r^2 = 0.99$ and 0.98 in parts a and b, respectively) to the experimental data.
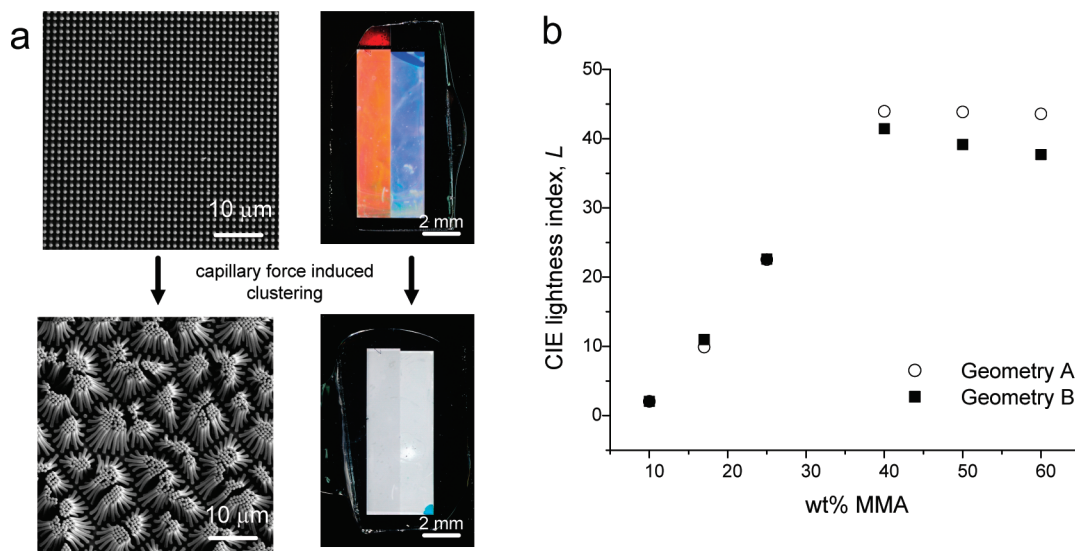
FIGURE 5. Whiteness caused by random clustering of the micropillar arrays and the corresponding CIE lightness index. (a) SEM (left) and optical (right) images of micropillar arrays before and after clustering. Two different colors in part a (top right) result from Bragg diffraction of micropillar arrays with different periodicities. (b) CIE lightness index of clustered micropillar arrays as a function of the MMA content.

lines in Figure 4 are linear fits to the experimental data, confirming the linear relationship between the cluster size and $1/E$. The slopes of the linear fit yield contact angle (θ) values of 72° for geometry A and 66° for geometry B, which are close to the measured value of 73° (Figure 2b) within experimental error. We note that for geometry A, however, we could have only three cluster size data because for PMMA content ≤40 wt % the cluster size was too large to have distinguishable clusters (Figure 1).

Whiteness of Clustered Micropillars. Finally, we investigated the optical effect of the capillary-force-induced clustering of a micropillar array as ultrathin whitening layers. Whiteness is important for many technologies such as the paper industry, coatings, textiles, and electronic displays. In these systems, the film thickness exceeds 100 μm, and whiteness is often enhanced by pigmentation or by fluorescent dyes. Nature, on the other hand, provides elegant examples of brilliant structural colors, such as those shown in the scales of white beetles, where their white color results from light scattering from random networks of microfilaments that are only a few micrometers thick (18). Before collapse, the micropillar arrays had angle-dependent colorful reflection due to Bragg diffraction of light from the highly ordered pattern (Figure 5a). After soaking in water and drying in air, however, the pillar array became randomly clustered and appeared white, which was attributed to random scattering of light (Figure 5a), similar to the phenomenon observed in the white beetle scales. We characterized the whiteness of the randomly clustered micropillar arrays in Figure 1 by measuring their CIE lightness index (24), L, using a photospectrometer (Figure 5b). For a low PMMA content, the micropillars ground-collapsed completely because of the low elastic modulus, resulting in low L. With an increase in the PMMA content, the pillars laterally collapsed into random clusters and L gradually increased. In general, the lightness index for geometry A was slightly higher than that for geometry B at the same composition

because A had larger cluster sizes than B. When the PMMA content was greater than 60 wt %, the micropillar arrays began to reappear colorful because of less collapse of the pillars. We observed a maximum lightness index L_{max} of ~45 for our structures, which were less than 9 μm thick (the micropillar height). In comparison, conventional uncoated paper has a lightness index of ~70 over 120-μm thickness. Although our clustered micropillar arrays are 33 % less white than the uncoated paper, the film thickness is 15 times thinner, which is important as a proof of concept for ultrathin structural whiteness. Possibilities to enhance the whiteness in the micropillar films are currently under investigation. $L > 80$ could be achieved by manipulating the micropillar materials and structures.

CONCLUSIONS

We studied the capillary-force-induced clustering of highly ordered polymeric micropillar arrays of well-defined geometries. By changing the composition of the water-swellable PHEMA versus glassy, nonswellable PMMA, we experimentally observed the effect of the elastic modulus on the micropillar cluster size. By minimizing the capillary and elastic bending energy, we estimated the average cluster size as a function of the pillar elastic modulus and geometry, which agreed well with the experimental values in general. Finally, we demonstrated the application of random clustering of micropillars for ultrathin (9 μm) whitening layers, mimcking the brilliant whiteness effect observed in ultrathin beetle scales, which contains randomly packed filaments (18). We believe that the presented mechanistic study of the hydrogel micropillar clustering under capillary force in this report will help pave the way for the rational design of structured hydrogels for applications that are dependent on the structural integrity.

Supporting Information Available: Elastic modulus measurement by AFM nanoindentation, an indentation force curve for a 60 wt % MMA sample, the corresponding $(z-d)$ versus $(d-d_0)^{1/2}$ plot, and numerical solution to equation 10. This material is available free of charge via the Internet at http://pubs.acs.org.

REFERENCES AND NOTES

(1) Jeong, H. E.; Lee, S. H.; Kim, J. K.; Suh, K. Y. *Langmuir* **2006**, *22*, 1640.

(2) Krupenkin, T. N.; Taylor, J. A.; Schneider, T. M.; Yang, S. *Langmuir* **2004**, *20*, 3824.

(3) Suh, K. Y.; Jon, S. *Langmuir* **2005**, *21*, 6836.

(4) du Roure, O.; Saez, A.; Buguin, A.; Austin, R. H.; Chavrier, P.; Siberzan, P.; Ladoux, B. *Proc. Natl. Acad. Sci. U.S.A.* **2005**, *102*, 2390.

(5) Tan, J. L.; Tien, J.; Pirone, D. M.; Gray, D. S.; Bhadriraju, K.; Chen, C. S. *Proc. Natl. Acad. Sci. U.S.A.* **2003**, *100*, 1484.

(6) Qu, L.; Dai, L.; Stone, M.; Xia, Z.; Wang, Z. L. *Science* **2008**, *322*, 238.

(7) Kaji, N.; Tezuka, Y.; Takamura, Y.; Ueda, M.; Nishimoto, T.; Nakanishi, H.; Horiike, Y.; Baba, Y. *Anal. Chem.* **2004**, *76*, 15.

(8) Pokroy, B.; Kang, S. H.; Mahadevan, L.; Aizenberg, J. *Science* **2009**, *323*, 237–240.

(9) Zhang, Y.; Lo, C. W.; Taylor, J. A.; Yang, S. *Langmuir* **2006**, *22*, 8595.

(10) Chandra, D.; Taylor, J. A.; Yang, S. *Soft Matter* **2008**, *4*, 979.

(11) Fan, J. G.; Dyer, D.; Zhang, G.; Zhao, Y. P. *Nano Lett.* **2004**, *4*, 2133.

(12) Tanaka, T.; Morigami, M.; Atoda, N. *Jpn. J. Appl. Phys.* **1993**, *32*, 6059.

(13) Chakrapani, N.; Wei, B.; Carrillo, A.; Ajayan, P. M.; Kane, R. S. *Proc. Natl. Acad. Sci. U.S.A.* **2004**, *101*, 4009.

(14) Segawa, H.; Yamaguchi, S.; Yamazaki, Y.; Yano, T.; Shibata, S.; Misawa, H. *Appl. Phys. A: Mater. Sci. Process.* **2006**, *83*, 447.

(15) Bico, J.; Roman, B.; Moulin, L.; Boudaoud, A. *Nature* **2004**, *432*, 690.

(16) Py, C.; Bastien, R.; Bico, J.; Roman, B.; Boudaoud, A. *Europhys. Lett.* **2007**, *77*, 44005.

(17) Kralchevsky, P. A.; Paunov, V. N.; Ivanov, I. B.; Nagayama, K. *J. Colloid Interface Sci.* **1992**, *151*, 79.

(18) Vukusic, P.; Hallam, B.; Noyes, J. *Science* **2007**, *315*, 348.

(19) Cappella, B.; Kaliappan, S. K.; Sturm, H. *Macromolecules* **2005**, *38*, 1874.

(20) Domke, J.; Radmacher, M. *Langmuir* **1998**, *14*, 3320.

(21) Dong, R.; Jensen, T. W.; Engberg, K.; Nuzzo, R. G.; Leckband, D. E. *Langmuir* **2007**, *23*, 1483.

(22) Sader, J. E.; Chon, J. W. M.; Mulvaney, M. *Rev. Sci. Instrum.* **1999**, *70*, 3967.

(23) Sneddon, I. N. *Int. J. Eng. Sci.* **1965**, *3*, 47.

(24) Wyszecki, G.; Stiles, W. S. *Color Science Concepts and Methods, Quantitative Data and Formulae*, 2nd ed.; John Wiley and Sons, Inc.: New York, 2000.

(25) Beer, F. B.; Johnston, E. R. *Mechanics of Materials*; McGraw-Hill, Inc.: New York, 1992.

(26) Zhao, Y. P.; Fan, J. G. *Appl. Phys. Lett.* **2006**, *88*, 103123.

AM900253Z